Robust mapping of electrical properties of graphene from terahertz time-domain spectroscopy with timing jitter correction

PATRICK R. WHELAN,[1] KRZYSZTOF IWASZCZUK,[2] RUIZHI WANG,[3] STEPHAN HOFMANN,[3] PETER BØGGILD,[1,4] AND PETER UHD JEPSEN[2,*]

[1]*DTU Nanotech, Technical University of Denmark, Ørsteds Plads Building 345C, DK-2800 Kongens Lyngby, Denmark*
[2]*DTU Fotonik, Technical University of Denmark, Ørsteds Plads Building 343, DK-2800 Kongens Lyngby, Denmark*
[3]*Department of Engineering, University of Cambridge, Cambridge CB3 0FA, United Kingdom*
[4]*Center for Nanostructured Graphene (CNG), Technical University of Denmark, Ørsteds Plads Building 345C, DK-2800 Kongens Lyngby, Denmark*
**puje@fotonik.dtu.dk*

Abstract: We demonstrate a method for reliably determining the electrical properties of graphene including the carrier scattering time and carrier drift mobility from terahertz time-domain measurements (THz-TDS). By comparing transients originating from directly transmitted pulses and the echoes from internal reflections in a substrate we are able to extract electrical properties irrespective of random time delays between pulses emitted in a THz-TDS setup. If such time delays are not accounted for they can significantly influence the extracted properties of the material. The technique is useful for a robust determination of electrical properties from terahertz time-domain measurements and is compatible with substrate materials where transients from internal reflections are well-separated in time.

© 2016 Optical Society of America

OCIS codes: (240.0310) Thin films; (300.6495) Spectroscopy, terahertz; (310.3840) Materials and process characterization; (310.6870) Thin films, other properties.

References and links

1. J. L. Tomaino, A. D. Jameson, J. W. Kevek, M. J. Paul, A. M. van der Zande, R. A. Barton, P. L. McEuen, E. D. Minot, and Y.-S. Lee, "Terahertz imaging and spectroscopy of large-area single-layer graphene," Opt. Express **19**, 141–146 (2011).
2. J. Horng, C. F. Chen, B. Geng, C. Girit, Y. Zhang, Z. Hao, H. A. Bechtel, M. Martin, A. Zettl, M. F. Crommie, Y. R. Shen, and F. Wang, "Drude conductivity of Dirac fermions in graphene," Phys. Rev. B - Condens. Matter Mater. Phys. **83**, 1–5 (2011).
3. I. Maeng, S. Lim, S. J. Chae, Y. H. Lee, H. Choi, and J. H. Son, "Gate-controlled nonlinear conductivity of Dirac fermion in graphene field-effect transistors measured by terahertz time-domain spectroscopy," Nano Lett. **12**, 551–555 (2012).
4. J. D. Buron, D. H. Petersen, P. Bøggild, D. G. Cooke, M. Hilke, J. Sun, E. Whiteway, P. F. Nielsen, O. Hansen, A. Yurgens, and P. U. Jepsen, "Graphene conductance uniformity mapping," Nano Lett. **12**, 5074–5081 (2012).
5. J. D. Buron, D. M. A. Mackenzie, D. H. Petersen, A. Pesquera, A. Centeno, P. Bøggild, A. Zurutuza, and P. U. Jepsen, "Terahertz wafer-scale mobility mapping of graphene on insulating substrates without a gate," Opt. Express **23**, 30721 (2015).
6. J. L. Tomaino, A. D. Jameson, M. J. Paul, J. W. Kevek, A. M. Van Der Zande, R. A. Barton, H. Choi, P. L. McEuen, E. D. Minot, and Y. S. Lee, "High-contrast imaging of graphene via time-domain terahertz spectroscopy," J. Infrared, Millimeter, Terahertz Waves **33**, 839–845 (2012).
7. M. J. Paul, J. L. Tomaino, J. W. Kevek, T. Deborde, Z. J. Thompson, E. D. Minot, and Y. S. Lee, "Terahertz imaging of inhomogeneous electrodynamics in single-layer graphene embedded in dielectrics," Appl. Phys. Lett. **101**, 2014–2017 (2012).
8. J. D. Buron, F. Pizzocchero, P. U. Jepsen, D. H. Petersen, J. M. Caridad, B. S. Jessen, T. J. Booth, and P. Bøggild, "Graphene mobility mapping," Sci. Rep. **5**, 12305 (2015).
9. C. Cervetti, E. Heintze, B. Gorshunov, E. Zhukova, S. Lobanov, A. Hoyer, M. Burghard, K. Kern, M. Dressel, and L. Bogani, "Sub-terahertz frequency-domain spectroscopy reveals single-grain mobility and scatter influence of large-area graphene," Adv. Mater. **27**, 2635–2641 (2015).

10. M. Scheller, C. Jansen, and M. Koch, "Analyzing sub-100-μm samples with transmission terahertz time domain spectroscopy," Opt. Commun. **282**, 1304–1306 (2009).
11. P. Kužel, H. Němec, F. Kadlec, C. Kadlec, P. Kuzel, H. Nemec, F. Kadlec, and C. Kadlec, "Gouy shift correction for highly accurate refractive index retrieval in time-domain terahertz spectroscopy," Opt. Express **18**, 15338–15348 (2010).
12. P. Braeuninger-Weimer, B. Brennan, A. J. Pollard, and S. Hofmann, "Understanding and controlling Cu catalyzed graphene nucleation: the role of impurities, roughness and oxygen scavenging," Chem. Mater. **28**, 8905-8915 (2016).
13. R. Wang, P. R. Whelan, P. Braeuninger-Weimer, S. Tappertzhofen, J. A. Alexander-Webber, Z. A. Van-Veldhoven, P. R. Kidambi, B. S. Jessen, T. J. Booth, P. Boggild, and S. Hofmann, "Catalyst interface engineering for improved 2D film lift-off and transfer," ACS Appl. Mater. Interfaces **8**, 33072–33082 (2016).
14. P. Blake, E. W. Hill, A. H. Castro Neto, K. S. Novoselov, D. Jiang, R. Yang, T. J. Booth, and A. K. Geim, "Making graphene visible," Appl. Phys. Lett. **91**, 63124 (2007).
15. J. D. Buron, F. Pizzocchero, B. S. Jessen, T. J. Booth, P. F. Nielsen, O. Hansen, M. Hilke, E. Whiteway, P. U. Jepsen, P. Bøggild, and D. H. Petersen, "Electrically continuous graphene from single crystal copper verified by terahertz conductance spectroscopy and micro four-point probe," Nano Lett. **14**, 6348–6355 (2014).
16. A. H. Castro Neto, F. Guinea, N. M. R. Peres, K. S. Novoselov, and A. K. Geim, "The electronic properties of graphene," Rev. Mod. Phys. **81**, 109–162 (2009).
17. M. M. Lucchese, F. Stavale, E. H. M. Ferreira, C. Vilani, M. V. O. Moutinho, R. B. Capaz, C. A. Achete, and A. Jorio, "Quantifying ion-induced defects and Raman relaxation length in graphene," Carbon **48**, 1592–1597 (2010).

1. Introduction

Terahertz time-domain spectroscopy (THz-TDS) is a non-contact measurement technique that can be used to determine electrical properties of conducting thin films such as graphene [1–4]. The non-contact approach is advantageous for in-line characterization and quality-control for industrial integration of graphene, especially when compared to standard field-effect measurements on graphene that require additional and intrusive fabrication steps for device processing. Non-gated rapid spatial mapping of the carrier drift mobility (μ_{drift}) and carrier density (N_s) of graphene by THz-TDS was recently reported [5], which presents a step forward compared to earlier reports which mainly gauges the conductivity [6,7] or extracts the mobility through back-gated THz-TDS measurements requiring special substrates [8,9].

An accurate and reliable determination of the electrical properties of graphene is required for THz-TDS to become an industry standard for rapid in-line characterization. In order to robustly determine the electrical properties such as μ_{drift} and N_s from non-gated measurements we would like to fit both the real and imaginary parts of the frequency dependent sheet conductivity to the Drude model. The electrical properties extracted from such fits were found to vary significantly depending on the choice of reference point on a sample. We attribute those point to point variations to time shifts (timing jitter and drift) between individual pulses transmitted in the setup. Various sources of possible artifacts from THz-TDS measurements have been identified and dealt with [10,11], but there are still no reports on a systematic correction for waveform to waveform timing jitter. Here we show a method for reliably extracting electrical properties from graphene by comparing the information that is available from transients that are directly transmitted through the substrate and transients originating from internal reflections in the substrate.

2. Methods

Chemical vapor deposited graphene was grown according to a published method [12] and subsequently transferred [13] onto high resistivity silicon with 90 nm SiO_2 for optical visibility of the graphene layer [14]. THz-TDS measurements were conducted using a commercial fiber-coupled spectrometer described in detail elsewhere [4]. Samples were raster

scanned with 200 μm step size in the focal plane of the THz beam to form spatial maps with ~300 μm resolution (at 1 THz).

An incident pulse leads to transients from a directly transmitted pulse and echoes from internal reflections in the substrate, see Fig. 1(a). The THz beam interacts strongly with free carriers in the graphene film [4,15] which means that the sheet conductivity of the graphene, $\tilde{\sigma}_s(f)$, can be extracted from the frequency-dependent complex transmission function $\tilde{T}_{film}(f) = \tilde{E}_{film}(f) / \tilde{E}_{sub}(f)$ where $\tilde{E}_{sub}(f)$ and $\tilde{E}_{film}(f)$ are the Fourier transforms of the THz waveforms transmitted through non-graphene covered Si and graphene covered Si, respectively. In the case of the directly transmitted pulse, the transmission function is

$$\tilde{T}^{(0)}_{film}(\omega) = \frac{\tilde{E}^{(0)}_{film}(\omega)}{\tilde{E}^{(0)}_{sub}(\omega)} = \frac{E_0 \tilde{t}_{film} \tilde{t}_{sub,air} e^{-i\delta}}{E_0 \tilde{t}_{air,sub} \tilde{t}_{sub,air} e^{-i\delta}} = \frac{\tilde{t}_{film}}{\tilde{t}_{air,sub}}, \tag{1}$$

where $\delta = \omega d \tilde{n}_{sub} / c$ is the phase and attenuation in a substrate with refractive index $\tilde{n}_{sub}$ and thickness d where c is the speed of light in vacuum and $\omega = 2\pi f$ is the angular frequency. The transmission coefficients t between air and substrate are calculated from the Fresnel equations $(\tilde{t}_{air,sub} = 2/(1+\tilde{n}_{sub}))$ while the transmission coefficient from air to substrate through a thin conducting film $\tilde{t}_{film}$ is given by $\tilde{t}_{film}(\omega) = 2/(\tilde{n}_{sub} + 1 + Z_0 \tilde{\sigma}_s(\omega))$ [1], where $Z_0 = 377\ \Omega$ is the vacuum impedance. The transmission function for the first internal reflection contains additional terms from internal reflections but is similar in structure.

For the directly transmitted pulse and the first reflected echo, $\tilde{\sigma}_s(\omega)$, is expressed as

$$\tilde{\sigma}^{(0)}_s(\omega) = \frac{1}{Z_0}\left(\frac{n_A}{\tilde{T}^{(0)}_{film}(\omega)} - n_A\right), \tag{2}$$

$$\tilde{\sigma}^{(1)}_s(\omega) = \frac{\pm n_A \sqrt{n_A^2 + 4n_A^2 n_B \tilde{T}^{(1)}_{film}(\omega) + 4n_B^2 \tilde{T}^{(1)}_{film}(\omega)} - n_A^2 - 2n_A n_B \tilde{T}^{(1)}_{film}(\omega)}{2n_B Z_0 \tilde{T}^{(1)}_{film}(\omega)}, \tag{3}$$

where $n_A = n_{Si} + 1$, $n_B = n_{Si} - 1$, and $n_{Si} = 3.417$. Electrical parameters such as the DC sheet conductivity, σ_{DC}, carrier scattering time, τ_{sc}, N_s, and μ_{drift} can be extracted after fitting $\tilde{\sigma}_s(\omega) = \sigma_1 + i\sigma_2$ to the Drude model

$$\tilde{\sigma}_s(\omega) = \frac{\sigma_{DC}}{1 - i\omega\tau_{sc}}.$$

σ_{DC} and τ_{sc} are determined directly from the fit to the Drude model as shown in Fig. 1(b), whereas N_s and μ_{drift} are evaluated from the relations [5]

$$N_s = \frac{\pi\hbar^2}{e^4 v_F^2}\left(\frac{\sigma_{DC}}{\tau_{sc}}\right)^2,$$

$$\mu_{drift} = \frac{\sigma_{DC}}{eN_s},$$

where v_F is the Fermi velocity with a value of 10^6 m/s [16]. The carrier density and drift mobility calculated from the fit in Fig. 1(b) is 2.25×10^{13} cm^{-2} and 1621.5 cm^2/Vs, respectively.

3. Results and discussion

A single layer film of graphene was transferred onto HR-Si/SiO_2 and spatially mapped by THz-TDS as shown in Fig. 1(c). The optical map shows that the graphene film is continuous. Fig. 1(d) shows how Raman mapping of the sample indicates a very low defect density in the graphene film as determined from the I(D)/I(G) peak intensity ratios with a mean I(D)/I(G) of 0.021 ± 0.019 [17].

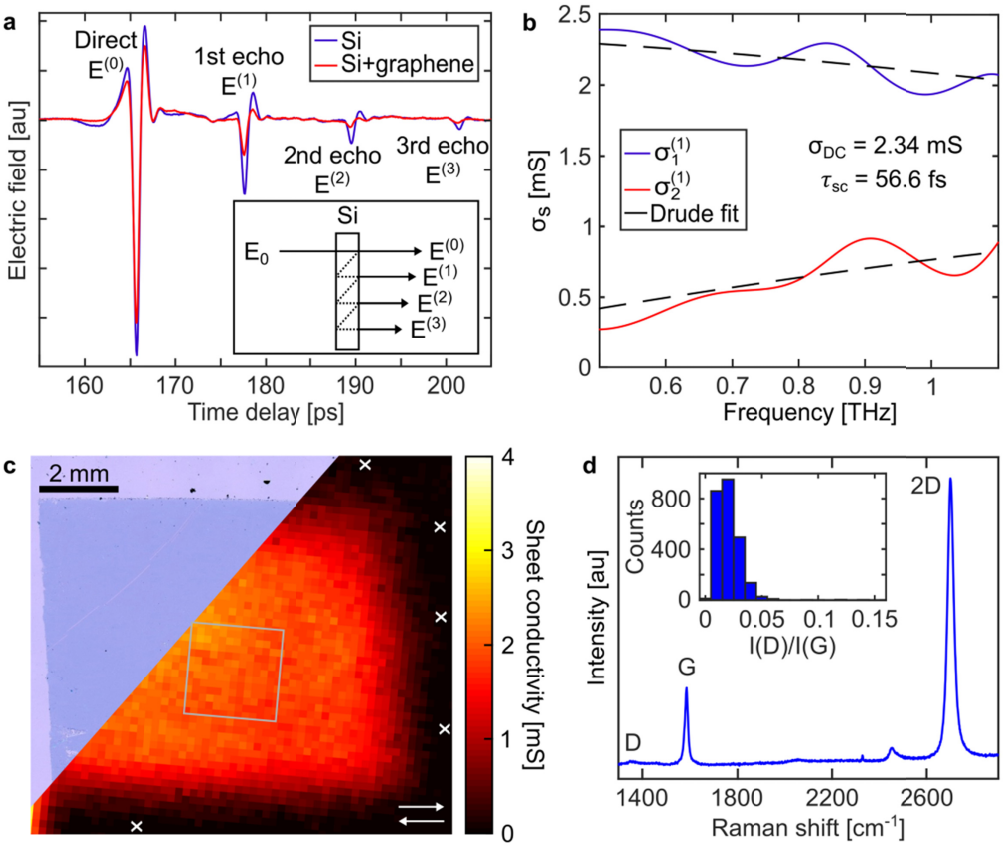

Fig. 1. (a) Waveform of THz pulses after transmission through a Si substrate without and with graphene. The inset shows how different echoes are generated by internal reflections in the substrate. (b) Sheet conductivity spectra for graphene on Si extracted from the first echo together with fits to the Drude model. (c) Optical map of the graphene sample combined with map of σ_1 from the directly transmitted pulse averaged from 0.8–0.9 THz. White arrows indicate the scanning direction during the THz-TDS measurement and the grey box illustrates the area chosen for performing timing jitter corrections. White crosses mark different areas used as sample reference points. (d) A representative Raman spectrum from the sample shown in c) with a histogram of Raman I(D)/(G) peak ratios in the inset.

Determination of $\tilde{\sigma}_s$ should yield the same result when extracted from the directly transmitted pulse or from any of the subsequent echoes. Since $\tilde{\sigma}_s$ depends on a measurement from a reference area compared to a sample area, it is sensitive to any variations between the two measurements such as substrate thickness variations or timing jitter. 10,000 waveforms with 100 averages per waveform were measured in our setup. Each waveform contains two distinct peaks as seen in the inset in Fig. 2(a) that were used to characterize timing jitter in the setup. The difference in time between the two peaks, t_p, and the arrival time of the first peak,

t_0, was obtained by fitting the individual peaks to Gaussian functions to extract the peak positions on the time axis. The arrival time of the first peak relative to the mean arrival time shows a spread in t_0 while the spread in t_p is more than ten times smaller as shown in Fig. 2(a). This indicates that it is the full waveforms that are shifted in time. The double peak character of the t_0 histogram has its origins in the THz-TDS instrument and is not within the scope of this paper. The variations in t_0 are on the order of few tens of femtoseconds, but even such small variations have significant influence on the electrical properties that are extracted from a graphene film. We note here that the timing jitter on the waveform arrival time is much smaller than the temporal step size of our commercial THz-TDS system (76 fs).

From the variation in arrival time at the sample for individual waveforms it follows that there might be a shift in time from the reference spectrum to the sample spectrum which will influence the determination of $\tilde{\sigma}_s$. Spectra of $\tilde{\sigma}_s$ for graphene on Si extracted from the directly transmitted pulse and from the first echo, respectively, do not overlap as shown in Fig. 2(b). The real parts, σ_1, follow each other while the imaginary parts, σ_2, have different slopes. This trend was observed for all the 169 pixels from the highlighted area in Fig. 1(c) being investigated.

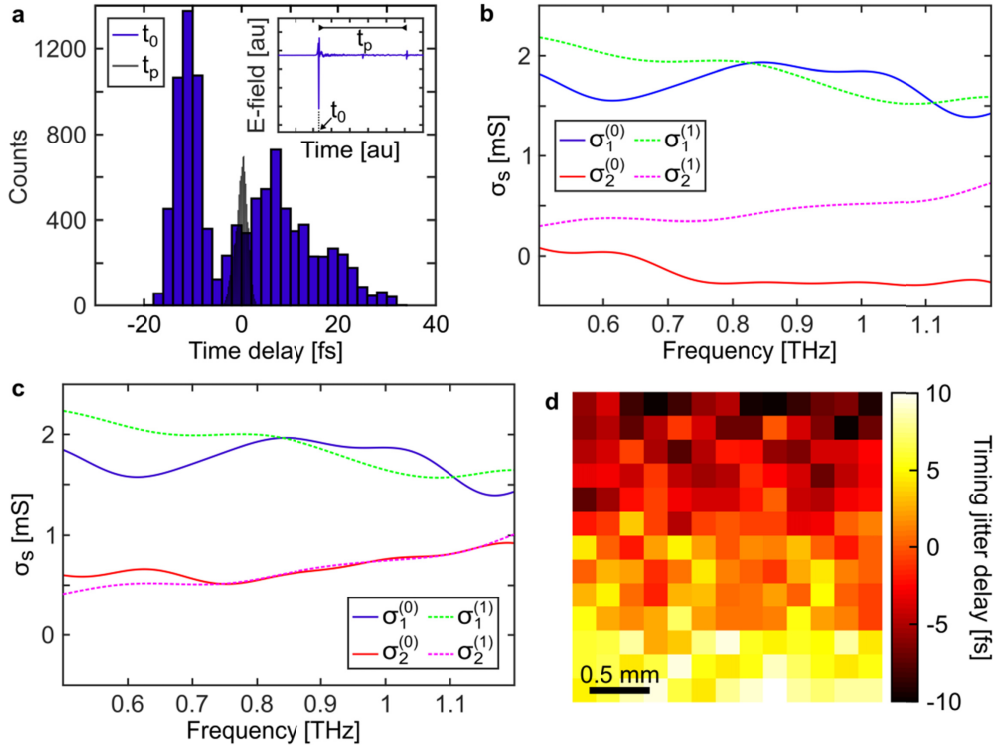

Fig. 2. (a) Time delay between individual waveforms measured in dry air. Inset shows one waveform. (b) Sheet conductivity spectra for graphene on Si extracted from the directly transmitted pulse and the first echo. (c) Sheet conductivity spectra from same pixel as (b) after correction for timing jitter. (d) Timing jitter delay in each pixel from the highlighted area in Fig. 1(c).

We take advantage of the fact that $\tilde{\sigma}_s$ should yield the same result when extracted from the directly transmitted pulse or from any of the subsequent echoes in order to correct for t_0 variations. We simultaneously calculate $\tilde{\sigma}_s^{(0)}$ and $\tilde{\sigma}_s^{(1)}$ while iteratively multiplying a phase

shift $e^{-i\Delta\delta}$ to $\tilde{E}_{film}$ in Eq. (1) in order to minimize the error between $\tilde{\sigma}_s^{(0)}$ and $\tilde{\sigma}_s^{(1)}$. The addition of a phase shift does not influence the magnitude of the signal, and will therefore mainly influence the imaginary part of $\tilde{\sigma}_s^{(0)}$ and $\tilde{\sigma}_s^{(1)}$. The resulting spectra after a correction corresponding to 4.2 fs are shown in Fig. 2(c) where both the real parts and the imaginary parts from the directly transmitted pulse and from the first echo now overlap. Fig. 2(d) shows a map of the time delay required to minimize the error between the spectra in each of the 169 pixels, where it is seen that the values are within the time delays measured between individual waveforms and that there is a noticeable continuous trend of time delay changes over time (scanning direction is horizontal with respect to the map).

In order to extract σ_{DC}, τ_{sc}, N_s, and μ_{drift} from the measurements, we fit $\tilde{\sigma}_s$ to the Drude model. This is usually done by only fitting to the real part of $\tilde{\sigma}_s$ [3,5,9]. Here, both real and imaginary parts of $\tilde{\sigma}_s^{(0)}$ and $\tilde{\sigma}_s^{(1)}$ are fitted to the Drude model (full fit) in each pixel that has been corrected for timing jitter in order to determine the electrical properties of the graphene film. The full fits after correction are compared to fits only to the real part of $\tilde{\sigma}_s$ (real-part fit) and to full fits to uncorrected data. Histograms of τ_{sc} and μ_{drift} acquired from fits to $\tilde{\sigma}_s^{(0)}$ using five different reference areas on the sample (highlighted as white crosses in Fig. 1(c)) are shown in Fig. 3.

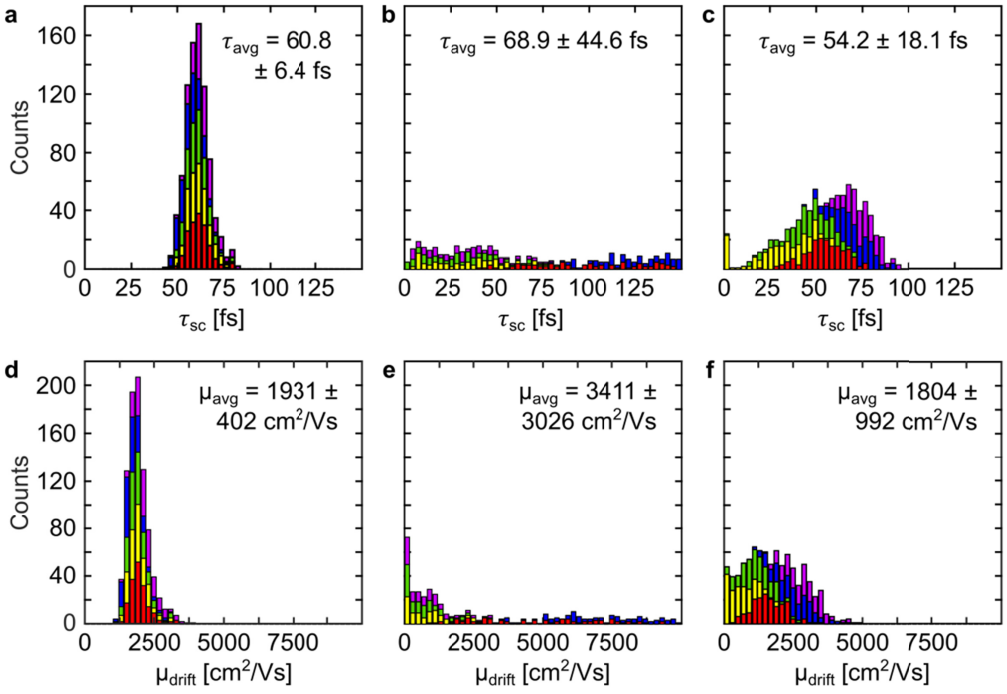

Fig. 3. Histograms of (a-c) τ_{sc} and (d-f) μ_{drift} for graphene extracted from the directly transmitted pulse from the area highlighted in Fig. 1(c). The five colors corresponds to properties calculated using five different reference areas on the sample, respectively and are plotted on top of each other. (a,d) Full fit after correction for timing jitter, (b,e) Full fit uncorrected, (c,f) Real-part fit after correction for timing jitter. Average values and standard deviations shown on plots cover all five data sets.

There are clear differences in the distributions extracted for τ_{sc} and μ_{drift} when comparing full fits after and before correction and real-part fits after correction. The data from different reference points generally falls on top of each other for both τ_{sc} and μ_{drift} when using full fits after correction, whereas full fits in the uncorrected case leads to a large spread in the determined properties of graphene. The big variations in τ_{sc} and μ_{drift} determined from full fits to uncorrected data are due to the changes in the slope of σ_2, which is highly sensitive to time differences between the pulse arriving at the reference and sample point, respectively. The average values obtained for real-part fits are in reasonable agreement (~10%) with the data from full fits after correction, but the extracted data from the five different reference points is more separated in this case, which leads to a larger uncertainty on the properties that are determined. Only real-part fits after correction are shown since σ_1 is negligibly affected by the timing jitter correction and the results from before correction are therefore similar to the results after correction in the case of real-part fits.

The comparison between electrical properties of graphene extracted from THz-TDS measurements by full and real-part fits using different reference points on the sample is expanded to cover σ_{DC}, τ_{sc}, N_s, and μ_{drift} extracted from both the directly transmitted pulse and the first echo which is shown in Fig. 4.

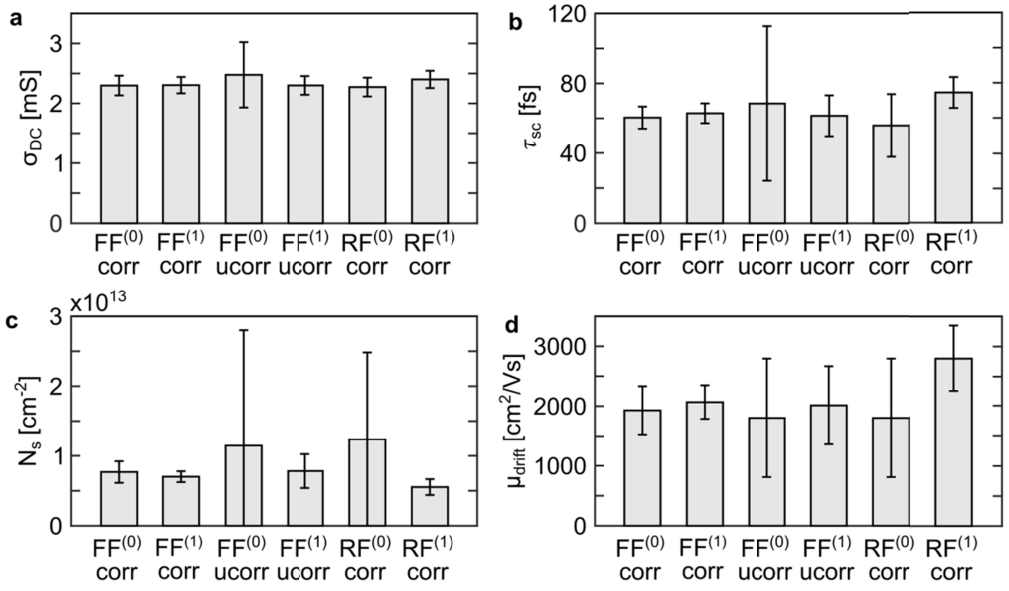

Fig. 4. Comparisons of electrical properties of graphene extracted from THz-TDS measurements using a full fit (FF) to the Drude model and only fitting to the real-part fit (RF) including non-corrected (ucorr) data and data after correction (corr) for timing jitter. (0) refers to data from directly transmitted pulses and (1) to the first reflected echo. (a) σ_{DC}. (b) τ_{sc}. (c) N_s. (d) μ_{drift}. The bars show the average value based on measurements from five different reference areas with error bars showing the standard deviation.

The average values from all fits are similar for σ_{DC} with some small variations for real-part fits and a large variation for the full fit to uncorrected data from the directly transmitted pulse. For τ_{sc}, N_s, and μ_{drift} the picture is different. Similar properties are extracted from full fits to $\tilde{\sigma}_s^{(0)}$ and $\tilde{\sigma}_s^{(1)}$ after correction for timing jitter. Without correction there are differences between the full fits to $\tilde{\sigma}_s^{(0)}$ and $\tilde{\sigma}_s^{(1)}$, and we also see an increase in the standard deviations due to variations between results from the different reference areas. We note that the average values obtained from full fits to uncorrected data for the first echo is similar to the values

obtained from full fits after jitter correction, however always with a larger standard deviation. A possible explanation for the difference between the uncorrected data from the directly transmitted pulse and the first echo could be the fact that the directly transmitted pulse has interacted less with the graphene film, thus having lower sensitivity compared to the first reflected echo.

There are differences between the values obtained from real-part fits to $\tilde{\sigma}_s^{(0)}$ and $\tilde{\sigma}_s^{(1)}$, since small variations in the slope of σ_1 will have a larger impact when the fit is not also dependent on σ_2. This shows that acquiring electrical properties by only fitting to the real part of $\tilde{\sigma}_s$ is generally less reliable compared to full fits to corrected data.

The results shown here highlights the importance of compensating for time delays during THz-TDS measurements due to both pulse-to-pulse timing jitter or long-time drift as there can be significant variations in the extracted electrical properties from a graphene film when using different reference areas on the same sample. We expect that this kind of compensation will be generally useful for all THz-TDS systems based on mechanical scanning of the time delay.

4. Conclusion

THz-TDS mapping measurements were conducted on graphene films. The determination of the electrical properties from the graphene film by full fits to the Drude model is extremely sensitive to small, unintentional time delays in the arrival time of pulses at the sample.

We have shown a robust and automated method for compensating for time delays between individual waveforms during THz-TDS measurements, which are for instance caused by any timing jitter and slow drift of the time delay scanning mechanics of the system. A small time shift is iteratively added to the sample time domain trace in order to minimize the difference between the frequency dependent sheet conductivity extracted from the directly transmitted pulse and that extracted from the first reflected echo. By applying such compensation, we are able to reliably extract the same electrical properties for the graphene film irrespective of the chosen reference point on a sample in a self-consistent and automated manner. Under realistic conditions we find that the correction is crucial in order to obtain meaningful statistics of the distribution of scattering times and mobility across a scanned area.

The method is expected to work for all conducting thin film materials where there are clear transients from a directly transmitted pulse and subsequent echoes that can be compared.

Funding

Innovation Fund Denmark (0603-005668B); Danish National Research Foundation (DNRF103); EU Horizon 2020 (696656); Danish Council for Independent Research (64092); EPSRC Doctoral Training Award (EP/M506485/1).